Atmos. Chem. Phys. Discuss., 8, 19123–19171, 2008
www.atmos-chem-phys-discuss.net/8/19123/2008/

Atmospheric Chemistry and Physics Discussions

This discussion paper is/has been under review for the journal *Atmospheric Chemistry and Physics (ACP)*. Please refer to the corresponding final paper in *ACP* if available.

Oxidation capacity of the city air of Santiago, Chile

Y. F. Elshorbany[1,2], R. Kurtenbach[1], P. Wiesen[1], E. Lissi[3], M. Rubio[3], G. Villena[3], E. Gramsch[4], A. R. Rickard[5], M. J. Pilling[6], and J. Kleffmann[1]

[1]Physikalische Chemie, FB C, Bergische Universität Wuppertal, Gaußstraße 20, 42119 Wuppertal, Germany
[2]Environmental Sciences Division, National Research Center, Dokki, Giza, Egypt
[3]Faculty of Chemistry and Biology, University of Santiago de Chile, USACH, Alameda L. Bernardo O'Higgins 3363, Santiago, Chile
[4]Physics Department, Faculty of Science, University of Santiago de Chile, Alameda L. Bernardo O'Higgins 3363, Santiago, Chile
[5]National Centre for Atmospheric Science, University of Leeds, Leeds, UK
[6]School of Chemistry, University of Leeds, Leeds, UK

Received: 8 July 2008 – Accepted: 21 September 2008 – Published: 14 November 2008

Correspondence to: J. Kleffmann (kleffman@uni-wuppertal.de)

Published by Copernicus Publications on behalf of the European Geosciences Union.

Abstract

The oxidation capacity of the highly polluted urban area of Santiago, Chile has been evaluated during an extensive summer measurement campaign carried out from 8–20 March 2005. The hydroxyl (OH) radical budget was evaluated employing a simple quasi-photostationary-state model (PSS) constrained with simultaneous measurements of HONO, HCHO, O_3, NO, NO_2, $j(O^1D)$, $j(NO_2)$, 13 alkenes and meteorological parameters. In addition, a zero dimensional photochemical box model based on the Master Chemical Mechanism (MCMv3.1) has been used to estimate production rates and total free radical budgets, including OH, HO_2 and RO_2. Besides the above parameters, the MCM model has been constrained by the measured CO and volatile organic compounds (VOCs) including alkanes and aromatics. Both models showed the same OH radical budget during daytime which indicates that the primary OH sources and sinks included in the simple PSS model are predominant. Mixing ratios of the main OH radical precursors were found to be in the range 0.8–7 ppbv (HONO), 0.9–11 ppbv (HCHO) and 0–125 ppbv (O_3). The alkenes average mixing ratio was ~58 ppbC accounting for ~12% of the total identified non-methane hydrocarbons (NMHCs). During the day time (8 h–19 h), HONO photolysis was shown to be the most important primary OH radical source comprising alone more than ~55% of the total initial production rate, followed by alkene ozonolysis (~24%) and photolysis of HCHO (~16%) and O_3 (~5%). The calculated average and maximum daytime OH production rates from HONO photolysis was 1.7 ppbv h^{-1} and 3.1 ppbv h^{-1}, respectively. Based on the experimental results a strong photochemical daytime source of HONO is proposed. A detailed analysis of the sources of OH radical precursors has also been carried out.

1 Introduction

The physical and chemical properties of the atmosphere are influenced by the presence of trace gases like nitrogen oxides (NO_x) and volatile organic compounds (VOCs).

ACPD

8, 19123–19171, 2008

The oxidising capacity of the atmosphere determines the rate of their removal, and hence controls the abundance of these trace gases. Understanding the processes and rates by which species are oxidized in the atmosphere is thus crucial to our knowledge of the atmospheric composition of harmful and climate forcing species. The term "oxidation capacity", OC is defined as the sum of the respective oxidation rates of the molecules Y_i (VOCs, CO, CH_4) by the oxidant X (X=OH, O_3, NO_3) (Geyer et al., 2001):

$$OC = \sum k_{Yi}[Y_i][X],$$

where k_{Yi} is the bi-molecular rate constant for the reaction of Y_i with X.

The hydroxyl radical (OH) is the primary oxidant in the atmosphere, responsible for the oxidation and removal of most natural and anthropogenic trace gases. In addition, initiating oxidation by reaction with the OH radical leads to the formation of harmful oxidants, such as ozone (O_3) and peroxyacetylnitrate (PAN). Thus, the identification and quantification of the different atmospheric OH radical sources and sinks is of paramount importance. Primary sources of the OH radical include the photolysis of ozone followed by the subsequent reaction of the excited O^1D atom with water, photolysis of formaldehyde (HCHO) in the presence of nitrogen oxide (NO), direct photolysis of nitrous acid (HONO) and the reactions of unsaturated hydrocarbons with O_3. Ren et al. (2003) recently calculated the relative importance of the above sources of OH in New York and estimated HONO photolysis contributed up to ~60%. In other field work studies, unexpected high daytime values of HONO were observed (e.g. Zhou et al., 2002; Kleffmann et al., 2002, 2005; Acker et al., 2006a, b) and new photochemical HONO sources have been proposed (Kleffmann, 2007), some of which have recently been identified in the laboratory (Zhou et al., 2003; George et al., 2005; Stemmler et al., 2006, 2007; Bejan et al., 2006; Li et al., 2008).

Summertime urban OH and HO_2 radical budgets have been evaluated in several field campaigns (e.g., George et al., 1999; Holland et al., 2003; Ren et al., 2003; Heard et al., 2004; Volkamer et al., 2007; Emmerson et al., 2007; Kanaya et al., 2007). In most of these studies, the experimental measurements were complemented with

model simulations in order to understand the chemical mechanisms that control tropospheric urban chemistry. Interestingly, the urban daytime OH and HO_2 radical budgets have been shown to be better simulated during the summer rather than winter, especially for high NO_x environments. Ren et al. (2006) used a box model incorporating the Regional Atmospheric Chemistry Mechanism, (RACM; Stockwell et al., 1997), which is based on the lumping technique to simulate radical budgets in New York during a winter campaign carried out in 2004 and obtained a median measured to model ratio of 0.98 for OH. However, the RACM model significantly underestimated HO_2, both during day and at night, with median measurement to model ratio of 6.0. Similarly, during the IMPACT campaign in Tokyo the RACM model reproduced wintertime OH well but underestimated the HO_2 by a median factor of 2. However, during the summer, the RACM model generally reproduced the daytime OH and HO_2 reasonably well (Kanaya et al., 2007). For Mexico City, Shirley et al. (2006) reported a median measured to model OH ratio of 1.07 during the morning and night and 0.77 during the rush hour using the RACM model. For HO_2, median measured to model ratios of 1.17, 0.79 and 1.27 were determined during the morning rush hour, midday and night, respectively. Besides lumped mechanisms, the more explicit Master Chemical Mechanism, MCM (http://mcm.leeds.ac.uk/MCM/; Jenkin et al., 1997; Saunders et al., 2003; Bloss et al., 2005) has been used extensively to interpret field measurements, carried out under a variety of conditions, including urban environments (e.g. Mihelcic et al., 2003; Emmerson et al., 2005a, b, 2007). During the BERLIOZ campaign, which took place in Berlin in August 1998 (Mihelcic et al., 2003), the hydroxyl and peroxy radical (RO_2) budgets have been measured and compared to those calculated by a photochemical box model containing the MCM. The modelled OH concentrations were found to be in excellent agreement with the measurements under high-NO_x conditions (NO_x>10 ppbv). The measured RO_2/HO_2 ratio was also well reproduced by the model. The MCM modelled radical concentrations during the TORCH campaign, which took place ~40 km NE of central London in the summer of 2003 also agreed well with measurements with only a 24% and 7% over prediction for OH and HO_2, respectively (Emmerson et al., 2007).

ACPD
8, 19123–19171, 2008

During the majority of the summer campaign studies reported in the literature the daytime peak in OH is well simulated, in the range of (3–10)×10^6 molecule cm^{-3} (Kanaya et al., 2007 and references therein). However, model OH production rate analysis has suffered from high uncertainties due to the use of estimated HONO concentrations rather than accurate direct simultaneous measurements (Heard et al., 2004; Emmerson et al., 2005b, 2007; Kanaya et al., 2007). Using MCM constrained box model with estimated HONO concentrations, the diurnally averaged OH concentrations during the summer of 1999 PUMA field campaigns in Birmingham city centre was underestimated by a factor of ∼2 during the day especially under high NO_x conditions (Emmerson et al., 2005a). This could be due to an underestimation of daytime HONO concentrations from using only known gas phase chemistry (Kleffmann et al., 2005). Thus, other photochemical sources have been proposed and recently identified in the laboratory, e.g. by the photochemical heterogeneous conversion of NO_2 on natural surfaces (George et al., 2005; Stemmler et al., 2006, 2007). It is worth noting that net average HONO contribution to radical budgets (defined as the HONO photolysis rate minus the radical loss rate due to the reaction OH+NO) of as low as 0% (Heard et al., 2004), and 3% (Emmerson et al., 2007; Kanaya et al., 2007) have been reported when HONO concentrations were only estimated. When the reaction of NO+OH was assumed as the unique HONO source, HONO was not a net source of OH radicals in the atmosphere (Heard et al., 2004). In other studies (Emmerson et al., 2005a, 2007) HONO formation was modelled using a heterogeneous rate constant, k_{het}, for the heterogeneous conversion of NO_2 on aerosol surfaces only. The rate constant was derived from the tunnel study by Kurtenbach et al. (2001), in which this reaction was studied on tunnel surfaces. An increase of the OH radical concentration by only 0.03% (Emmerson et al., 2005) and a net contribution of HONO to the radical production by 3% during hot and stagnant conditions (Emmerson et al., 2007) were calculated. A similar contribution of 3% was estimated assuming heterogeneous production of HONO by dry deposition of NO_2 to the ground with HONO subsequently produced according to the reaction $2NO_2+H_2O \rightarrow HONO+HNO_3$ (Kanaya et al., 2007). During the LAFRE campaign in

California, 1993 (George et al., 1999), a significant reduction in both modelled OH and HO_2 has been observed when heterogeneous HONO formation on ground surfaces was removed from the model especially in the morning hours. Similarly, in BERLIOZ, the RACM model predicted only 50% of the measured OH concentrations when HONO photolysis was switched off in the early morning (04:00–08:00 UT) (Alicke et al., 2003). It is clear, therefore, from results reported from several recent field studies (e.g. Ren et al., 2003; Kleffmann et al., 2003; Acker et al., 2006a, b), that the simultaneous measurement of HONO, along side other major radical precursors, is crucial in the analysis of atmospheric radical budgets.

Several studies focusing on air quality issues in Santiago de Chile have shown that severe air quality problems, including the photochemical formation of large amounts of ozone, PAN and related photooxidants, have a significant impact on health problems in the city (Rappenglück et al., 2000; Rubio et al., 2004; Rappenglück et al., 2005). However, none of these studies have observed the diurnal variation of the important OH radical precursor HONO.

The work reported here focuses on the analysis of a comprehensive suite of data taken during a summertime field campaign carried out in the city of Santiago de Chile from 8–20 March 2005. This work constitutes the first detailed evaluation of photochemistry in Santiago, Chile that takes into account all the major primary OH radical sources, namely the photolysis of HONO, formaldehyde (HCHO) and ozone (O_3) and the dark reactions of ozone with alkenes, in addition to peroxy radical (HO_2 and RO_2) recycling reactions. Under the high NO_x conditions often experienced in Santiago, a constrained photochemical box model based around the MCM and a simple photostationary steady state (PSS) model were used to evaluate radical budgets and their source apportionment during late summer in order to understand the photochemistry occurring in such a highly polluted urban environment as Santiago.

ACPD
8, 19123–19171, 2008

2 Methodology

2.1 Measurement site

The measurements were performed downtown of the city of Santiago, Chile, on the third floor of the Physics Department of the University of Santiago (USACH) and in the Park O'Higgins station (POH), situated ~1.8 km southeast of the main USACH measurement site. The city of Santiago de Chile is located at –33.45° latitude and 70.67° longitude ~550 m above sea level and surrounded by two mountain ranges, the Andes and the Cordillera de la Costa.

2.2 Measurement techniques

The techniques used to measure the different parameters are listed in Table 1 with their response times and detection limits. At the USACH site HONO was measured by the sensitive LOPAP (Long Path Absorption Photometer) technique (Heland et al., 2001; Kleffmann et al., 2002). The LOPAP instrument was recently intercompared against the DOAS technique, both in a smog chamber and in the urban atmosphere. Excellent agreement was obtained under daytime photochemical smog conditions (Kleffmann et al., 2006), in contrast to other intercomparison studies (e.g., Appel et al., 1990; Spindler et al., 2003). The excellent agreement can be explained by the active correction of interferences and the use of an external sampling unit, minimizing artefacts in sampling lines. Potential heterogeneous HONO formation on the walls of the USACH building on which the sampling unit was fixed (ca. 130 cm distance), was also investigated. No significant variation of the HONO concentration was observed when varying the distance of the sampling unit (20–150 cm) from the wall.

Other measured parameters at the USACH site included HCHO, NO, NO_2, PAN and photolysis frequencies $j(NO_2)$ and $j(O^1D)$. The photolysis frequencies of HCHO and HONO were calculated from the measured $j(NO_2)$ and $j(O^1D)$ data (Holland et al., 2003). O_3, CO and meteorological data were obtained from the POH station. C_3-

C_{10} NMHCs were sampled at the USACH site on adsorption tubes and analyzed by GC-FID analysis following the US EPA Compendium Method TO-17 (see Table 2). The detailed analytical procedure is published elsewhere (Niedojadlo et al., 2007). The ambient NMHCs have been sampled using an automatic system equipped with calibrated regulated flow controllers and applying an air flow of 20 ml/min on the adsorbing tubes. After sampling, the adsorption tubes were capped with Parafilm, stored in air sealed glass tubes in the refrigerator and returned to Germany for GC-FID analysis. Potential ozone interferences have been tested in the laboratory by sampling a standard VOC mixture over the same type of adsorption tubes with and without addition of ozone at a mixing ratio of 135 ppbv. Sampling periods of three hours were chosen using NMHCs mixing ratios corresponding to the minimum observed NMHCs mixing ratios during the measurement campaign. Ozone was prepared by passing a regulated flow of pure synthetic air through a mercury UV-lamp based ozoniser followed by a reaction vessel with glass rings cooled with dry ice to 203 K in order to trap the HO_x radicals from the ozonised air. Ozone has been monitored by a commercial UV absorption based monitor (Table 1). Only reductions of as low as –8.8% for trans-2-butene and as high as –29.4% for *cis*-2-pentene were observed. However, since average and maximum ozone mixing ratios of 20 ppbv and 126 ppbv were observed during the measurement campaign, we exclude significant negative interferences from ozone. This result is in agreement with the study of Koppmann et al. (1995) who found no significant interferences from ozone up to mixing ratios of 100 ppbv either using pressurized air samples or cryogenically collected air samples even at very low VOC concentrations.

2.3 Modelling approach

2.3.1 Simple quasi-photostationary state model, PSS

OH concentrations were calculated with the steady-state approximation using the radical production rates from HONO, HCHO and ozone photolysis, alkenes ozonolysis and the radical loss rate. Under the prevailing high NO_x conditions radical loss is

ACPD
8, 19123–19171, 2008

mainly governed by the reactions of OH with NO_x (cf. George et al., 1999; Ren et al., 2006; Emmerson et al., 2005b, 2007; Kanaya et al., 2007). During the day, formation of HONO by reaction of OH with NO is essentially balanced by photolysis of HONO formed from this reaction. Radical removal by peroxy-peroxy radical reactions is unimportant under high NO_x conditions (see Sect. 3.3). Thus, the *net* radical loss rate can be estimated from the rate of reaction of OH with NO_2:

$$L_R = k_{NO2+OH}[NO_2][OH]$$

The applied steady state approximation can be summarized as follows:

$$P_R = L_R.$$

The total rate of radical initiation, P_R, is given by:

$$\begin{aligned} P_R &= \text{new OH} - k_{OH+NO}[NO][OH] + \text{new HO}_2, \text{ for which :} \\ \text{new OH} &= j(HONO)[HONO] + j(O^1D)[O_3]\Phi_{OH} + \Sigma k_{O3+alkene}[alkene][O_3]\Phi_{OH}, \\ \text{new HO}_2 &= 2j(HCHO_{radical})[HCHO]. \end{aligned}$$

For ozone photolysis Φ_{OH} (defined here as the fraction of O^1D produced that will react with H_2O rather than is quenched to ground state O^3P) was calculated using known rate constants for O^1D quenching and reaction with water in addition to the measured water concentration. For the alkene ozonolysis reactions Φ_{OH} represents the OH yield from the respective reactions (e.g. Rickard et al., 1999).

Therefore, the steady state OH concentration is given by:

$$[OH]_{PSS} = P_R/(k_{NO2+OH}[NO_2]).$$

2.3.2 The Master Chemical Mechanism, MCM

A zero dimensional photochemical box model based on the Master Chemical Mechanism, MCMv3.1 (http://mcm.leeds.ac.uk/MCM) has been used to evaluate the radical

budgets. MCMv3.1 is a near-explicit chemical mechanism describing the detailed gas phase tropospheric degradation of methane and 135 primary emitted NMHCs, which leads to a mechanism containing ca. 5900 species and 13 500 reactions. The mechanism is constructed according to a set of rules as defined in the latest mechanism development protocols (Jenkin et al., 1997; Saunders et al., 2003; Bloss et al., 2005). The MCM photochemical box model's system of simultaneous stiff ordinary differential equations (ODEs) was integrated with a variable order Gear's backward differentiation method (FACSIMILE; Curtis and Sweetenham, 1987). The model was constrained with average 10 min values of the following measured parameters: $j(NO_2)$, $j(O^1D)$, relative humidity, pressure, temperature, NO, NO_2, HONO, CO, HCHO, O_3, PAN and 31 NMHCs (see Table 2). j(HONO) and $j(HCHO_{radical})$ where parameterized from the measured $j(NO_2)$ and $j(O^1D)$ (Holland et al., 2003) and their values have been constrained in the model. The other photolysis frequencies are parameterized within the model using a two stream isotropic scattering model under clear sky summertime conditions (Hayman, 1997; Saunders et al., 2003). The photolysis rates are calculated as a function of solar zenith angle and normalized by a scaling factor, calculated from the ratio of measured and model calculated $j(NO_2)$ values, which takes into account the effects of varying cloud cover. A series of rate of production analyses (ROPA) were carried out in order to identify the most important photochemical processes driving the formation and loss of OH and HO_2. The MCM photochemical model was run for a period of five days, with the model being constrained with the same measured campaign average parameters each day, in order to generate realistic concentrations for the unmeasured intermediate species. By the fifth day the free radicals in the model have reached a photostationary state, which has been used for the data evaluation.

3 Results and discussion

3.1 Measurements results analysis

For the data evaluation, all measurements were averaged over 10 min time intervals. The trace gases data of the whole campaign are shown in Fig. 1 while the 10 min average diurnal variation profiles are shown Fig. 2a. During the campaign sunny weather conditions were prevailing with temperatures ranging from 285 K to 305 K during the daytime. The wind speed was relatively low ranging from 0.2 m s^{-1} to 4.1 m s^{-1}, and the average relative humidity was 49%, reaching up to 100% during the night. The maximum HONO mixing ratio during rush hour reached ~7 ppbv on the 10 March at ~9 h. For the campaign averaged data maximum and minimum HONO mixing ratios of 3.7 ppbv at around 8 h and 1.5 ppbv around 17 h were obtained. For CO and NO a similar rush hour peak at ~9 h on the 10 March was also observed with maximum concentrations of 3.6 ppmv and 480 ppbv, respectively.

The average daytime rush hour maxima for CO and NO were 1.38 ppmv and 180 ppbv, respectively (see Fig. 2a). The NO_2 maximum was shifted later owing to small direct emissions and formation by the reaction of NO with peroxy radicals and O_3. From the slope of the correlation plot of HONO against NO_x a mean HONO/NO_x ratio of 0.008 was estimated during the rush hour peaks, which is in excellent agreement with direct tunnel measurements in Europe (Kurtenbach et al., 2001).

PAN, HCHO and O_3 showed typical diurnal variations with average daytime maxima at about 14 h of 3 ppbv, 7 ppbv and 65 ppbv, respectively, demonstrating their photochemical formation. However, from the fast increase of HCHO in the early morning, when the O_x (NO_2+O_3) increase was still small, a significant contribution from direct emissions was also identified (see Sect. 3.8.1). In addition to the maximum at ca. 14 h, the ozone diurnal variation profile is characterized with an afternoon shoulder at 18 h, which has become a typical feature under photochemical smog conditions in Santiago (Rappenglück et al., 2000, 2005). The daytime HONO concentrations are significantly higher than in other polluted urban areas such as New York, Milan or Rome, where the

ACPD
8, 19123–19171, 2008

minimum mean daytime concentrations were 0.3–0.6 ppbv (Ren et al., 2003; Kleffmann et al., 2006; Acker et al., 2006b). The high mixing ratios and the daytime maximum of the HONO/NO_x ratio (see Fig. 2b) in Santiago points to a very strong daytime HONO source.

53 measured NMHCs have been identified (see Table 2). The remaining 127 unidentified NMHCs represents in average about 43% of the total measured NMHCs. Total average measured NMHCs of ~900 ppbC and known average measured NMHCs of ~490 ppbC were determined, which correspond to average diurnal VOC/NO_x ratios of 14 and 7, respectively. According to the VOC/NO_x ratio rule (Sillman, 1999) the first value corresponds to a NO_x-sensitive photochemical regime while the second corresponds to a VOC-sensitive photochemical regime. However, the VOC/NO_x ratio may not correctly represent the sensitivity of a photochemical regime. An explicit VOC-NO_x-O_3 sensitivity analysis showed that the photochemical regime in Santiago is clearly VOC sensitive (Elshorbany et al., 2008). Alkanes have the highest contribution (ppbC) to NMHCs (56%) followed by aromatic hydrocarbons (32%) and finally alkenes (12%). The BTEX compounds (benzene, toluene, ethylbenzene and xylenes) contribute ~80% of the total aromatic hydrocarbons and ~25% of the total NMHCs.

3.2 Oxidation capacity

The loss rate of the VOCs and CO due to reactions with OH, O_3 and NO_3 has been calculated using the MCM model. The average oxidation capacity of OH, O_3 and NO_3 radicals through the entire day was 3.7×10^7, 4.3×10^6 and 1.2×10^5 molecule cm^{-3} s^{-1} representing 89.4, 10.3 and 0.3% of the total oxidation capacity, respectively. Clearly, the OH radical was the dominant oxidant during daytime reaching a maximum of 3.2×10^8 molecules cm^{-3} s^{-1} corresponding to about 94% of the total oxidation capacity at about 15 h. The ozone contribution to the oxidation capacity during daytime ranged from 6% to 11% while it reached >50% during the night, mainly due to alkene ozonolysis. In general, the nitrate radical had a negligible contribution during both the day and at night, which was mainly caused by the high NO concentrations during the campaign.

The modelled NO_3 concentrations showed two peaks of 1.0×10^6 molecules cm^{-3} at about 13 h and of 8.4×10^5 molecules cm^{-3} at 19 h. The total number of the depleted molecules per day due to oxidation by OH, O_3 and NO_3 were 6.4×10^{12}, 7.4×10^{11} and 2.0×10^{10} molecules cm^{-3}, respectively. Accordingly, the OH radical is the driving force of the oxidation capacity of the atmosphere in Santiago and thus, only the sources and sinks of the OH radical are further considered in this study.

3.3 Radical production and destruction rates

The total production and destruction rates of OH and HO_2 calculated by the MCM model constrained to campaign averaged data are shown in Fig. 3a with the ratios of the radical production/destruction shown in Fig. 3b. The ratio was around unity throughout the day for the hydroperoxy radical whilst the ratio for the hydroxyl radical reaches a maximum of ~1.7 during the morning similar to that observed in other urban studies (Mihelcic et al., 2003; Shirley et al., 2006; Sheehy et al., 2008), which is caused by the photolysis of night time accumulated HONO.

The high total production and destruction rates are dominated by the recycling reactions of peroxyradicals (RO_2+NO and HO_2+NO). The main loss of RO_2 is due to its reaction with NO with an average daytime loss rate of ~34.6 ppbv h^{-1}, which accounts for most of the HO_2 production. The next most important HO_2 sources are the reactions of OH with CO and HCHO with average daytime production rates of ~0.5 and ~1.1 ppbv h^{-1}, respectively. HCHO photolysis accounts for the new HO_2 (see Sect. 2.2.1) with an average daytime production rate of 0.54 ppbv h^{-1} (Figs. 4b and 5). In contrast to the other secondary oxygenated VOCs (OVOCs), HCHO is considered here as a net source of HO_2 (new OH_2) since on average only 28% of the HCHO is formed photochemically (see Sect. 3.8.1). The main destruction route of HO_2 is through its reaction with NO reaching rates up to 71 ppbv h^{-1}, with a daytime average of ~28.4 ppbv h^{-1} which corresponds to ~90% of the total destruction rate, and is comparable to those of the TORCH, ~99% (Emmerson et al., 2007) and BERLIOZ

ACPD
8, 19123–19171, 2008

campaigns, >80% (Mihelcic et al., 2003). The loss rates due to the HO_2 self-reaction and its cross-reactions with RO_2 are very small with daytime averages of <0.01 and 0.02 ppbv h^{-1}, respectively, in agreement with other urban studies (e.g., George et al., 1999; Ren et al., 2006). The main OH loss route is through its reaction with hydrocarbons, followed by reactions with NO and NO_2. The rates of OH destruction due to hydrocarbons oxidation depend on the detailed chemical mechanism and can be estimated using the following relationships:

$$L_{OH}(OH + VOC) \approx L_{OH}(total) - k_{NO2+OH}[NO_2][OH] - k_{OH+NO}[NO][OH] \quad (1)$$

or

$$L_{OH}(OH + VOC) \approx \sum k_i[VOC_i][OH] \quad (2)$$

where L_{OH} (total) is the total loss rate as calculated by the MCM model and k_i represents the bimolecular rate constant for OH reaction with the corresponding VOC.

If Eq. (2) is used to calculate L_{OH} due to reactions with the measured VOCs only, the OH loss rate will be underestimated since reactions with secondary VOC products are not included. Consequently, HO_2 as a source of OH will be over estimated. Relationship (1) takes into account the detailed degradation of the VOCs due to reactions with OH, as calculated by the MCM photochemical box model, which includes the secondary VOC oxidation products. The average daytime (8 h–19 h) loss of OH radicals by VOC reaction calculated employing Eq. (2) is about 6 ppbv h^{-1} while that obtained using Eq. (1) is about 28.4 ppbv h^{-1}, representing about 79% of the total OH loss. The fraction of OH loss by VOC reactions is similar to that of Berlin, 50–70% (Mihelcic et al., 2003) and Mexico City, 72% (Shirley et al., 2006).

OH production is dominated by the recycling reaction of HO_2 with NO, $P_{OH}(HO_2 \rightarrow OH)_{recycled}$ for which:

$$P_{OH}(HO_2 \rightarrow OH)_{recycled} = P_{OH}(HO_2 \rightarrow OH) - HO_2 \text{ new},$$

ACPD
8, 19123–19171, 2008

where:

$P_{OH}(HO_2 \rightarrow OH) = k_{HO2+NO}[HO_2][NO]$.

$P_{OH}(HO_2 \rightarrow OH)_{recycled}$ reached a maximum production rate of 70.5 ppbv h^{-1} with a daytime average of ~27.8 ppbv h^{-1} (Fig. 4a). The $P_{OH}(HO_2 \rightarrow OH)$ route accounts for ~80% of the total OH radical production. This value is comparable to that estimated during TORCH, 80% (Emmerson et al., 2007) and BERLIOZ, >70% (Mihelcic et al., 2003) and Mexico City, >80% (Shirley et al., 2006 and Sheehy et al., 2008). The oxidation of hydrocarbons results however in the production of other radical precursors namely, O_3 and HCHO as by-products in addition to alkene ozonolysis as a subsequent process. These processes, in addition to HONO photolysis, constitute the net radical production term, P_R (Fig. 4a). The rest of the OH production term (1.1 ppbv h^{-1}) is mainly due to the ozonolysis of the secondary alkenes produced from the oxidation process which are not constrained by the measurements (see Fig. 5). The balance between $P_{OH}(HO_2 \rightarrow OH)_{recycled}$ and L_{OH} (OH+VOC) (see Sect. 3.5), results in the NO_2+OH (termination) reaction becoming the net dominant sink for OH with a maximum loss rate of 6.4 ppbv h^{-1} and a daytime average loss rate of ~3.4 ppbv h^{-1} (see Fig. 5). An accompanying sensitivity analysis showed that only under very low NO_x conditions reaching three orders of magnitude lower than the current levels (i.e. ~0.1 ppbv NO) HO_2 recycling through its reaction with NO could be a limiting factor (Elshorbany et al., 2008). Under these conditions hydrocarbon oxidation could be a net sink for OH radicals, which in turn will also lead to a reduction in the OH sources, i.e. O_3 and HCHO photolysis as well as alkenes ozonolysis.

3.4 OH reactivity

The OH reactivity defined as the reciprocal of the OH radical lifetime has been calculated as L_{OH}(total)/[OH]. The mean day average modelled OH reactivity is about 42 s^{-1} reaching a maximum of 105 s^{-1} during rush hour (Fig. 4c) and a night-time peak of

$60\,s^{-1}$. These numbers are slightly higher than the average and night-time peaks measured in Mexico City of 25 and $35\,s^{-1}$, respectively, while the maximum measured OH reactivity in Mexico City of $120\,s^{-1}$ exceeded that of Santiago (Shirley et al., 2006). Sheehy et al. (2008) have also reported a modelled total reactivity of $110\,s^{-1}$ during the morning rush hour and 45–50 s^{-1} at night in Mexico City. Both, Ren et al. (2006) and Yoshino et al. (2006) reported OH reactivities in the range of 10–100 s^{-1} in New York City and Tokyo, respectively. The diurnal variation of the modelled OH reactivity (Fig. 4c) is characterized by morning rush hour and night peaks in agreement with studies of Ren et al. (2006) and Shirley et al. (2006). Underestimation of the OH reactivity using relationship (2) has been previously observed when compared with measured OH reactivity in different field measurements (Di Carlo et al., 2004; Yoshino et al., 2006; Ren et al., 2006 and references therein). It is worth mentioning that the OH uptake on aerosol surfaces and the uncertainty of the rate coefficient of ($k_{(NO2+OH)}$) could not account for the missing OH reactivity in previous field measurements (Yoshino et al., 2006; Ren et al., 2006).

3.5 Radical propagation

Although hydrocarbon oxidation consumes most of the OH radicals (L_{OH}(OH+VOC)=28.4 ppbv h^{-1} on average), it also regenerates these radicals through the secondary production of OH, P_{OH} (sec.), (28.9 ppbv h^{-1}) given by the sum of $P_{OH}(HO_2 \rightarrow OH)_{recycled}$ (27.8 ppbv h^{-1}) and other secondary sources of 1.1 ppbv h^{-1} (mainly, secondary alkenes+O_3, see Fig. 5). This result is in good agreement with the study of Emmerson et al. (2007) for which a similar balance was reported for stagnant "heat wave" periods during TORCH 2003, which were associated with high pollutant concentrations, low wind speed and high temperatures, which is probably similar to the situation in Santiago. On the contrary, for lower pollutant concentrations, $OH \rightarrow RO_2$ and $HO_2 \rightarrow OH$ were not balanced (Emmerson et al., 2007).

While all the measured hydrocarbons were quantified, not all could be defined (see

Sect. 3.1). In addition, not all defined hydrocarbons could be included in the MCM model because either some of these compounds were measured as a mixture of two compounds (or more) or not defined in the MCM (see Table 2). Thus, to further investigate the recycling process, an additional MCM model scenario has been run, in which the concentrations of all aromatic hydrocarbons and alkanes in addition to isoprene and propene have been increased by a factor of 2 while the rest of alkenes have been left unchanged. The reason for including only isoprene and propene is because of their relatively high reactivity with OH but their low potential for OH production through ozonolysis (see Sect. 3.8.2). Only ~1% increase in the modelled OH concentration was observed for this additional scenario. In addition, although the fluxes $P_{OH}(HO_2 \rightarrow OH)_{recycled}$ and $L_{OH}(OH+VOC)$ increased by almost a factor of 2, they were still balanced. These results clearly demonstrate that the main net radical sources and sinks were not affected by the VOC level and that the secondary radical sources (e.g. OVOC photolysis) and sinks (e.g. $RONO_2$) are included in the recycling process, i.e. do not add to the net initiation sources or termination reactions. In the main, this can be explained by the high NO concentrations during daytime in Santiago and the fast recycling through the reactions RO_2+NO and HO_2+NO.

The high recycling efficiency of the peroxy radicals can be demonstrated by the relatively low HO_2/OH ratio evaluated by the MCM model (see Fig. 6a). The low maximum in the HO_2/OH ratio of ~11 is typical for highly polluted conditions (e.g. Mihelcic et al., 2003) and implies a high recycling efficiency towards OH. The RO_2/HO_2 ratio (Fig. 6b) of 1–1.5 is similar to that reported in Berlin with a maximum modelled ratio of 1.3 (Mihelcic et al., 2003) but much lower than that of 3.9 calculated for the TORCH campaign (Emmerson et al., 2007). While the RO_2/HO_2 and HO_2/OH ratios both reach a minimum in the morning at about 9 h, the HO_2/OH ratio reaches its afternoon maximum at about 14:30 h when the NO levels reach a minimum. The average daytime maximum HO_2 radical concentration of 6.3 pptv (see Fig. 7a) is very similar to that measured in Tokyo, 2004 (Kanaya et al., 2007). The average daytime maximum total peroxy radical concentration of 15 pptv is relatively low when compared with other studies (Mihelcic

et al., 2003; Shirley et al., 2006) and can be explained by the high NO concentrations in the city of Santiago. This is also in agreement with the expected anti-correlation between the HO_2/OH ratio and NO as shown in Fig. 7b in agreement with other studies (e.g. Emmerson et al., 2007 and references therein).

3.6 Net radical sources

Evaluation of the total rates of radical initiation and termination required a simple steady state approach (see Sect. 2.2.1) that takes into account only the net radical sources and sinks. The net photolysis of HONO, HCHO, ozone and the reactions of ozone with alkenes are considered as initiation reactions while reaction of the OH radical with NO_2 is the main termination reaction. According to this assumption, the radical production rates, P_R, of the main corresponding species were evaluated with the same rate constants used in MCMv3.1. The average absolute and relative diurnal contributions to radical production are shown in Fig. 8a and b respectively. For daytime conditions (8 h–19 h) HONO photolysis has by far the highest contribution of ~55% followed by alkenes ozonolysis (~24%), HCHO photolysis (~16%) and ozone photolysis (~5%).

The high relative contribution of HONO is in excellent agreement with other recent studies (Ren et al., 2003, 2006; Kleffmann et al., 2005; Acker et al., 2006a, b), in which an integrated contribution of up to 56% was reported. For average daytime conditions (8 h–19 h), high net mean and maximum OH production rates by HONO photolysis of 1.7 ppbv h^{-1} and 3.1 ppbv h^{-1}, respectively, have been determined, the latter being even higher than the ~2 ppbv h^{-1} reported by Ren et al. (2003) for New York City. Only in the study of Acker et al. (2006b) was a higher maximum OH production rate by HONO photolysis of up to 6 ppbv h^{-1} reported for the city of Rome. However, this number is an upper limit since in their estimations the back reaction of NO+OH was not considered. During the morning, for which the maximum production rate was reported by Acker et al. (2006b), high NO concentrations can especially lead to a strong overestimation of net OH production rates (see Sect. 3.8.3). On a 24-h basis, HONO photolysis was also the dominant radical source contributing ~52% to P_R followed by

alkene ozonolysis, ~29%, HCHO photolysis ~15% and ozone photolysis ~4%. During almost the entire daytime the HONO photolysis contribution was higher than any other primary source except in the early evening when the contribution from alkene ozonolysis starts to dominate. This is caused by the decreasing light intensity with the ozone concentrations remaining high. In the early morning, the photolysis of HONO is the dominant source representing ~80% of the total radical budget. This is due to its low dissociation energy threshold and the high concentrations accumulated during night-time.

A high morning peak production rate that slows down during the day has been previously observed in Los Angeles, Milan, Pabstthum (downwind of Berlin) and Mexico City (George et al., 1999; Alicke et al., 2002, 2003; Volkamer et al., 2007, respectively). However, in contrast to these studies, where the net OH production was very low in the afternoon, the relative contribution of the OH production by HONO photolysis never falls below 40% for Santiago (see Fig. 8b). This high daytime contribution of HONO is in good agreement with other recent studies under urban conditions (Ren et al., 2003; Acker et al., 2006b). The reason for the difference between the two sets of studies in which the contribution of HONO to afternoon radical production is either significant or negligible is still unclear. One potential explanation would be an overestimation of HONO due to interferences and sampling artefacts for all studies, in which wet chemical instruments were used (see Kleffmann and Wiesen, 2008). However, the LOPAP instrument used in the present study corrects for interferences and was successfully validated against the DOAS technique in a recent urban study in Milan (Kleffmann et al., 2006). In addition, a simple PSS analysis of the HONO data from the Milan campaign showed that HONO was also a strong net source of OH radicals during daytime, a result confirmed by the parallel co-located DOAS measurements (Kleffmann et al., 2006). This result is in contradiction to other DOAS measurements carried out at the same place under similar meteorological conditions and time of the year (Alicke et al., 2002). The reason for this difference is still unclear. Another explanation for the different daytime contributions of HONO in different studies may be the different sampling

altitudes and strong vertical gradients during daytime. However, in the study of Alicke et al. (2002) the light path of the DOAS was even lower than the sampling height during the present study and no gradients were observed during daytime (Stutz et al., 2002). In addition, in the present study no horizontal gradients were observed towards the wall of the building on which the external sampling unit was fixed, excluding strong local wall sources. In conclusion, the reason for the different daytime contribution of HONO to the OH production remains unclear. The high contribution of HONO observed in the present study may be explained by the unique geographical situation of Santiago under very high pollution levels.

The average diurnal variation of the OH concentration calculated by both the MCM and PSS models are shown in Fig. 9. The maximum estimated OH concentrations of 1.4×10^7 molecules cm^{-3} occurs approximately one hour after the maximum in $j(O^1D)$. Using different simplified photo-stationary state approaches, Rappenglück et al. (2000) and Rubio et al. (2005) estimated much lower values of $\sim2.6\times10^6$ and $\sim8.8\times10^6$ molecules cm^{-3}, respectively. Reasons for theses differences are that Rappenglück et al. (2000) did not consider HONO photolysis and alkenes ozonolysis while Rubio et al. (2005) did not consider alkenes ozonolysis.

The excellent agreement between the OH concentration profiles evaluated by both the MCM and PSS models shows that the major OH radical sources and sinks are included in the PSS model and that the sinks $OH\rightarrow RO_2$ are balanced with the sources $RO_2\rightarrow OH$.

3.7 Correlation of OH with $j(O^1D)$ and $j(NO_2)$

In spite of the complexity of the mechanisms controlling OH concentrations, the OH correlation with $j(O^1D)$ has shown to have a linear pattern in both urban and rural environments and for long and short time periods (Rohrer et al., 2006). For Santiago, the calculated OH radical concentration also correlates well with $j(O^1D)$ (R^2=0.54), and $j(NO_2)$ (R^2=0.56). An even stronger correlation between the daytime OH and $j(NO_2)$ has been also obtained in other studies (e.g. Kanaya et al., 2007 and references

therein). In addition, a better correlation between the total rate of radical initiation, P_R, and $j(NO_2)$ compared to the correlation with $j(O^1D)$ was observed in the present study, especially for low j-values in the morning and evening (see Fig. 10a and b). This can be explained by the much broader diurnal profile of $j(NO_2)$ compared to $j(O^1D)$. The results demonstrate the importance of the UV-A rather than UV-B region for the production of OH during daytime which is dominated by the daytime production of HONO.

3.8 Source apportionments of the main OH radical precursors

3.8.1 Formaldehyde (HCHO) contribution

HCHO is a main photochemical oxidation precursor contributing ~16% of the total primary radical sources, P_R, during the day time in Santiago. HCHO is both primarily emitted and produced photochemically from the oxidation of VOCs (Friedfeld et al., 2002; Garcia et al., 2006). In this study, we have used O_3 and NO_x as HCHO tracers for which NO_x has been assumed as an indicator for primary HCHO resulting from direct emissions and O_3 as a photochemical indicator. The measured HCHO was described by:

$$[HCHO]_{measured} = \beta_o + \beta_1 \times [O_3] + \beta_2 \times [NO_x]$$

where β_o is the background HCHO (BKG), and the factors β_1 and β_2 are the average weighted slopes of HCHO to O_3 and NO_x, respectively. For the whole campaign, values of β_1=0.062 and β_2=0.018 ppbv/ppbv, respectively were determined. The photochemically formed HCHO (PHOT) comprises up to >70% of the observed HCHO in the afternoon (Fig. 11a). In contrast, during the early morning rush hour the primary HCHO (traffic) comprised up to 90% (Fig. 11a). Averaged on a daily basis, ~34% of the measured HCHO is due to direct emissions while photochemical and background HCHO account for ~28 and ~38%, respectively. The value of the direct emitted fraction is very similar to the 32±16% previously reported by Rubio et al. (2006) while the sum

of the photochemical and background fractions is similar to the secondary fraction reported during the summer in Santiago, 79±23% (Rubio et al., 2006) and London, 74% (Harrison et al., 2006). Since only 28% of the HCHO is photochemically formed as a result of hydrocarbon oxidation, HCHO was considered as a net source of HO_2 (new OH_2) in the present study.

Photochemical HCHO production has also been simulated using the MCMv3.1 photochemical box model constrained with all measured trace gases including the NMHCs except the measured HCHO. The photochemical HCHO calculated using O_3 as tracer matched well that calculated by the MCM model with a gap in the late afternoon (see Fig. 11b). This gap however, is due to the afternoon ozone shoulder, which has become a typical feature during photochemical smog episodes in Santiago de Chile (Rappenglück, 2000, 2005). Primary HCHO starts to build up in the early morning at about 6:30 h, nearly one hour before sunrise, and becomes the dominant source until ~9 h. The photochemical formation of HCHO follows the light intensity, and starts to increase nearly an hour after the sunrise, becoming dominant at around ~13 h and reaching a maximum at ~16 h nearly 3 h after the maximum in $j(NO_2)$. The photochemical HCHO contribution starts to decline at ~19 h, about 3 h after the $j(NO_2)$ starts decreasing, while the primary HCHO turns again to be the dominant source until 2 h due to night time emissions. The average background baseline of HCHO is less than 2 ppbv representing about 20% of the total HCHO throughout the day (Fig. 11a), which is in agreement with other studies (Garcia et al., 2006). However, unpredicted high background concentrations of HCHO, reaching a maximum of up to 5 ppbv at ~10 h, have been evaluated. One explanation is an underestimation of photochemical produced HCHO by the use of O_3 as tracer, since photochemical formed O_3 is first efficiently titrated by the morning rush-hour NO. In this case, photochemical HCHO would become even more important after ~9 h. The use of O_x (O_3+NO_2) as tracer was not possible, since NO_2 is also linked to direct emissions. Another explanation for the high HCHO background peak may be direct HCHO emissions that are not traced by NO_x (Garcia et al., 2006). These emissions should then however, be limited to the time period 9 h–14 h

ACPD
8, 19123–19171, 2008

(see Fig. 11a), which is unreasonable. Finally, the high background HCHO could also be caused by mixing of surface air masses with the residual layer in the morning when the boundary layer height is increasing. The concentration of HCHO in the residual layer could remain high from the previous day. Rappenglück et al. (2005) has also observed a similar background carbonyl peak at noontime in Santiago.

The contribution of each of the VOC classes (alkenes, alkanes, aromatics) to the photochemically formed formaldehyde has been determined by the MCM model. As expected, the alkenes are the dominant photochemical precursor contributing alone by more than 70%, followed by aromatics, 18%, and alkanes, 12%. These contributions are in good agreement with those reported in Mexico (Volkamer et al., 2007). Of the alkenes, oxidation of isoprene contributes alone about 23% to the photochemical produced HCHO, propene 11% and α-pinene 9%. From the aromatics class, 1,3,5-trimethylbenzene represents 6% followed by *ortho*-xylol, 4%, and toluene, 3%. Of the alkanes, 2-metylbutane, decane and 3-methylpentane are the major sources contributing to about 3%, 2% and 1.6% respectively. OH is the dominant oxidant responsible for nearly 85% of the total HCHO produced by the oxidation of hydrocarbons followed by alkene ozonolysis, 14%. The contribution of NO_3 was found to be negligible.

3.8.2 Alkenes ozonolysis contributions

Unlike the other OH radical sources, alkene ozonolysis can occur at night as well as during the day (Paulson and Orlando, 1996; Johnson and Marston, 2008). In this study, the ozonolysis of alkenes was found to be the second most important radical initiation source after HONO photolysis, accounting for 29% of the OH formed on 24-h basis. Although their total concentrations are only ~19% of the total measured alkenes, internal alkenes contribute 86% to the total alkene OH radical production and nearly 21% to the total primary radical production, P_R, as shown in Fig. 12a. The order of efficiency in OH production from the reactions of ozone with alkenes is:

internal alkenes > cycloalkenes > terminal alkenes.

Among the internal alkenes, 2-methyl-2-butene and 2,3-dimethyl-2-butene have the highest contributions to the alkenes OH radical production with 37% and 33%, respectively (see Fig. 12b). Cycloalkenes are represented by α-pinene alone and contribute about 6.6% to the total alkene concentration, ~9% to total alkene OH production and ~2% to P_R. The other measured cycloalkenes are not yet included in the MCM. Terminal alkenes, while representing 75% of the alkenes concentration, contribute only ~5% to the total alkene OH production rate and about 1% to P_R (Fig. 12a).

3.8.3 Contribution of HONO during daytime

As already discussed, over the last few years it has been demonstrated that the contribution of nitrous acid to the primary radical production, P_R, has been frequently underestimated (e.g. Ren et al., 2003 ; Kleffmann et al., 2005; Acker et al., 2006a). High measured daytime concentrations point to an additional strong HONO source (Kleffmann, 2007), for which several photochemical reactions have recently been proposed from laboratory studies (Zhou et al., 2003; George et al., 2005; Bejan et al., 2006; Stemmler et al., 2006, 2007).

The photostationary state concentration of HONO, $[HONO]_{PSS}$, was calculated from the known gas phase chemistry by the following equation:

$$[HONO]_{PSS} = k_{OH+NO}[OH][NO]/(j(HONO) + k_{OH+HONO}[OH]).$$

On average, $[HONO]_{PSS}$ was found to account for about 69% of the observed HONO concentration reaching its maximum contribution during the rush hour peak time at ~10 h coinciding with the NO peak. During the early afternoon (12:30 h–15 h), when the absolute production rate of OH by HONO photolysis was highest, the PSS contributed on average ~66% of the measured HONO. Thus, one reason for the extreme high HONO daytime concentrations observed is the daytime production of HONO by the gas phase reaction of NO+OH caused by the very high levels of OH and NO. However, this reaction and the uncertainty in the PSS concentration by only gas phase chemistry (see below) cannot explain the measured daytime values of HONO alone.

ACPD
8, 19123–19171, 2008

If the heterogeneous dark conversion of NO_2 (see Sect. 3.8.4) is included, the PSS increases by only 4% during noon, thus, an additional daytime source of HONO is needed. The most important uncertainty in the calculation of the PSS concentration besides the measured [NO], [HONO] and j(HONO) values is modelled [OH]. However, an average maximum OH concentrations of 2.2×10^7 molecules cm^{-3}, which is about 155% of the modelled OH, is required to get $[HONO]_{PSS}$ equal to measured values. The OH simulated by the MCM model was validated through different field intercomparisons and showed excellent agreement with that measured, especially under such high NO_x conditions (Mihelcic et al., 2003; Sheehy et al., 2008). Recently, Sheehy et al. (2008) reported maximum OH over prediction by the MCM of 20% during afternoon. In contrast, for Santiago an under prediction of the modelled OH level by ca. 55% would be necessary to explain the daytime concentrations of HONO. Therefore, additional average daytime HONO sources of 1.7 ppbv h^{-1} are necessary. These additional daytime HONO sources become obvious from the diurnal variation of the $HONO/NO_x$ ratio (Fig. 2b). While the night-time behaviour, with a linear increase of the $HONO/NO_x$ ratio from 2–5%, is typical for urban conditions and can be explained by known emission and heterogeneous conversion of NO_2 on ground surfaces (Alicke et al., 2002; Kleffmann et al., 2002, 2003; Vogel et al., 2003), the second daytime maximum, reaching almost 8%, has not been observed in our previous urban studies in such a pronounced manner. A daytime maximum under urban conditions was however observed for the city of Rome (Acker et al., 2006b) and is also typical for remote and mountain site measurements (see e.g., Huang et al., 2002; Kleffmann et al., 2002; Acker et al., 2006a, Kleffmann and Wiesen, 2008). A daytime maximum in the $HONO/NO_x$ ratio can only be explained by a very strong additional photochemical HONO source. Three mechanisms were identified recently, two of them being well correlated to $j(NO_2)$ (George et al., 2005; Bejan et al., 2006; Stemmler et al., 2006, 2007), while the photolysis of nitric acid (Zhou et al., 2003) would better correlate to $j(O^1D)$, caused by the much lower wavelength range of the nitric acid photolysis. This was tested using the experimental data by plotting the net production rate of OH radicals due to HONO photolysis against

$j(NO_2)$ and $j(O^1D)$. Both plots ($j(NO_2)$, R^2=0.62 and $j(O^1D)$, R^2=0.45) show that the daytime source is correlated with the light intensity, confirming former assumptions. However, since a better correlation was obtained when $j(NO_2)$ was used, especially for low j-values, the heterogeneous conversion of NO_2 on photosensitized organics (George et al., 2005; Stemmler et al., 2006, 2007) and gas phase photolysis of organic nitrogen compounds (e.g. nitrophenols, Bejan et al., 2006) may be of higher importance compared to the nitric acid photolysis in Santiago. Similar results were obtained when plotting P_R against $j(NO_2)$ and $j(O^1D)$ (see Fig. 10 and Sect. 3.7).

3.8.4 HONO dark sources

Besides photochemical daytime sources of HONO, formation of HONO during the night by heterogeneous conversion of NO_2 on humid surfaces is well known (Alicke et al., 2002). The dark heterogeneous rate constant of HONO formation, k_{het}, due to the first order conversion of NO_2 on humid surfaces ($NO_2 + X \rightarrow HONO$) has been estimated from the increase of the $HONO/NO_2$ ratio during the night (see also Alicke et al., 2002). An average k_{het} of $(3.5\pm1.9)\times10^{-6}\,s^{-1}$ has been obtained, which is similar to that of $(3.3\pm1.4)\times10^{-6}\,s^{-1}$ obtained by Alicke et al. (2002). This heterogeneous rate constant has been found to correlate inversely with the wind speed (R^2=0.65) confirming heterogeneous formation on ground surfaces during the night (Kleffmann et al., 2003). However, almost no correlation of k_{het} with relative humidity was observed (R^2=0.086) in contrast to the study by Stutz et al. (2004). The lack of water dependence can be explained by the heterogeneous conversion of NO_2 into HONO on adsorbed organics (Arens et al., 2002; Gutzwiller et al., 2002; Ammann et al., 2005), which are persistent on any urban surfaces. For this type of reactions only a moderate humidity dependence was observed in the laboratory (Arens et al., 2002) for a humidity range comparable to the present study. In addition, NO_2 conversion on organic surfaces is much faster than the typical proposed reaction of NO_2 with water on surfaces (Finlayson-Pitts et al., 2003) at atmospheric NO_2 levels and thus is a more reasonable source for night-time

formation of HONO in the atmosphere.

4 Conclusions

The oxidising capacity of the atmosphere over the urban area of Santiago, Chile, has been studied for the first time during an extensive measurement campaign in the summer 2005. A zero dimensional photochemical box model containing the detailed gas phase mechanism MCMv3.1 was constrained with a suite of ancillary measurements including HONO, HCHO, O_3, NO_x, PAN, VOCs, $j(O^1D)$, $j(NO_2)$ and meteorological parameters. The average ratio of total production/destruction rates of the hydroperoxy radical (HO_2) was around unity throughout the day, whilst the production/destruction ratio for the hydroxyl radical (OH) reaches a maximum of ~1.7 during the morning. HO_2 radical production was dominated by the RO_2+NO reaction while HO_2 destruction was dominated by its reaction with NO, which was also the strongest OH source (~80%). OH loss was dominated with its reaction with hydrocarbons (~79%). The high recycling efficiency was demonstrated by the low HO_2/OH ratio of ~11. The RO_2/HO_2 ratio of 1–1.5 is comparable to that of other urban studies. Both, the MCM and simple PSS models predict the same OH concentrations showing that the main radical precursors included in the PSS model are dominant and that the OH→RO_2 sinks are balanced by the RO_2→OH sources. This balance was verified by an additional MCM model scenario that was run under a different VOC reactivity regime. The high modelled OH concentrations show that the high daytime concentrations of HONO cannot be explained by known gas phase chemistry and suggest the presence of an additional strong daytime source of HONO. This conclusion is further supported by the observations of a second daytime maximum in the HONO/NO_x ratio. HONO was the most important direct OH source with daytime average contribution of 55% followed by alkenes ozonolysis, 24%, HCHO photolysis, 16%, and O_3 photolysis, 5%. The better correlation of the daytime HONO source with $j(NO_2)$ compared to $j(O^1D)$ shows that daytime HONO formation cannot be explained by the recently proposed nitric acid

ACPD
8, 19123–19171, 2008

photolysis channel. Alkene ozonolysis represented the second most important direct source of OH radicals with internal alkenes contributing ~86% to the OH radical formation. HCHO source apportionment has been achieved using NO_x and O_3 as direct emission and photochemical tracers, respectively. Photochemical HCHO comprises up to >70% of the observed HCHO during the afternoon. The HCHO photochemical source apportionment has revealed that alkenes contribute most by 70% followed by aromatics, 18%, and alkanes, 12%. The major contribution of HONO to the direct OH radical production is in good agreement with several recent studies and highlights the importance of HONO measurements in studies which focus on the radical chemistry of the atmosphere.

Acknowledgement. Financial support by the German Academic Exchange Service (DAAD) under contract no. ale-03/23601 and FONDECYT (Project 1040032 and 1085007) is gratefully acknowledged. Y. Elshorbany would like to thank Roberto Sommariva, Earth System Research laboratory, NOAA, Boulder, US for supplying the python scripts used for the ROPA calculations. We also would like to thank Birger Bohn, Forschungszentrum Jülich, Germany for the calibration of the $j(NO_2)$ filter radiometer. Thanks are given to the Physics Department, Faculty of Science, USACH, for the use of their facilities during the field campaign.

References

Acker, K., Möller, D., Wieprecht, W., Meixner, F. X., Bohn, B., Gilge, S., Plass-Dülmer, C., and Berresheim H.: Strong Daytime Production of OH from HNO_2 at a Rural Mountain Site, Geophys. Res. Lett., 33, L02809, doi:10.1029/2005GL024643, 2006a.

Acker, K., Febo, A., Trick, S., Perrino, C., Bruno, P., Wiesen, P., Möller, D., Wieprecht, W., Auel, R., Guisto, M., Geyer, A., Platt, U., and Allegrini, I.: Nitrous Acid in the Urban Area of Rome, Atmos. Environ., 40, 3123–3133, 2006b.

Alicke, B., Platt, U., and Stutz, J.: Impact of nitrous acid photolysis on the total hydroxyl radical budget during the Limitation of Oxidant Production/Pianura Padana Produzione di Ozono study in Milan, J. Geophys. Res., 107(D22), 8196, doi:10.1029/2000JD000075, 2002.

Alicke, B., Geyer, A., Hofzumahaus, A., Holland, F., Konrad, S., Pätz, H. W., Schäfer, J., Stutz,

J., Volz-Thomas, A. and Platt, U.: OH formation by HONO photolysis during the BERLIOZ experiment, J. Geophys. Res. 108(D4), 8247, doi:10.1029/2001JD000579, 2003.
Ammann, M., Rössler, E., Strekowski, R., and George, C.: Nitrogen Dioxide Multiphase Chemistry: Uptake Kinetics on Aqueous Solutions Containing Phenolic Compounds, Phys. Chem. Chem. Phys., 7, 2513–2518, 2005.
Appel, B. R., Winer, A. M., Tokiwa, Y., and Biermann, H. W.: Comparison of Atmospheric Nitrous Acid Measurements by Annular Denuder and Optical Absorption Systems, Atmos. Environ., 24A, 611–616, 1990.
Arens, F., Gutzwiller, L., Gäggeler, H. W., and Ammann, M.: The Reaction of NO_2 with Solid Anthrarobin (1,2,10-trihydroxy-anthracene), Phys. Chem. Chem. Phys. 4, 3684–3690, 2002.
Bejan, I., Abd El Aal, Y., Barnes, I., Benter, T., Bohn, B., Wiesen, P., and Kleffmann J.: The Photolysis of Ortho-Nitrophenols: A new Gas Phase Source of HONO. Phys. Chem. Chem. Phys., 8, 2028–2035, 2006.
Bloss, C., Wagner, V., Bonzanini, A., Jenkin, M. E., Wirtz, K., Martin-Reiejo, M., and Pilling, M. J.: Evaluation of detailed aromatic mechanisms (MCMv3 and MCMv3.1) against environmental chamber data, Atmos. Chem. Phys. 5, 623–639, 2005.
Curtis, A. R. and Sweetenham, W. P.: FACSIMILE/CHEKMAT users manual, Rep. AERER12805, Her Majesty's Stn. Off Norwich, UK, 1987.
Di Carlo, P., Brune, W. H., Martinez, M., Harder, H., Lesher, R., Ren, X., Thornberry, T., Carroll, M. A., Young, V., Shepson, P. B., Riemer, D., Apel, E., and Campbell, C.: Missing OH reactivity in a forest: Evidence for unknown reactive biogenic VOCs, Science, 304, 722–725, 2004.
Elshorbany, Y., Wiesen, P., Kleffmann, J., Kurtenbach, R., Rubio, R., Lissi, E., Villena, G., Rickard, A. R., and Pilling M. J.: Explicit analysis and simulation of the ozone photochemical episode in Santiago, Chile, in preparation, 2008.
Emmerson, K. M., Carslaw, N., Carpenter, L. J., Heard, D. E., Lee, J. D., and Pilling, M. J.: Urban atmospheric chemistry during the PUMA campaign 1: Comparison of modelled OH and HO_2 concentrations with measurements, J. Atmos. Chem., 52, 143–164, 2005a.
Emmerson, K. M., Carslaw, N., and Pilling, M. J.: Urban Atmospheric Chemistry during the PUMA Campaign. 2: Radical budgets for OH, HO_2 and RO_2, J. Atmos. chem., 52, 165–183, 2005b.
Emmerson, K. M., Carslaw, N., Carslaw D. C., Lee, J. D., McFiggans, G., Bloss, W. J., Gravestock, T., Heard, D. E., Hopkins, J., Ingham, T., Pilling, M. J., Smith, S. C., Jacob, M., and

Monks, P. S.: Free radical modelling studies during the UK TORCH Campaign in summer 2003, Atmos. Chem. Phys., 7, 167–181, 2007, http://www.atmos-chem-phys.net/7/167/2007/.

Finlayson-Pitts, B. J., Wingen, L. M., Sumner, A. L., Syomin, D., and Ramazan, K. A.: The Heterogeneous Hydrolysis of NO_2 in Laboratory Systems and in Outdoor and Indoor Atmospheres: An Integrated Mechanism, Phys. Chem. Chem. Phys., 5, 223–242, 2003.

Friedfeld, S., Fraser, M., Ensor, K., Tribble, S., Rehle, D., Leleux D., and Tittel, F.: Statistical analysis of primary and secondary atmospheric formaldehyde, Atmos. Environ., 36, 4767–4775, 2002.

Garcia, A. R., Volkamer R., Molina L. T., Molina M. J., Samuelson J., Mellqvist J., Galle B., Herndon S. C., and Kolb C. E.: Separation of emitted and photochemical formaldehyde in Mexico City using a statistical analysis and a new pair of gas-phase tracers, Atmos. Chem. Phys., 6, 4545–4557, 2006, http://www.atmos-chem-phys.net/6/4545/2006/.

George, L. A., Hard, T. M., and O'Brien R. J.: Measurement of free radicals OH and HO_2 in Los Angeles smog, J. Geophys. Res., 104(D9), 11 643–11 656, 1999.

George, C., Strekowski, R. S., Kleffmann, J., Stemmler, K., and Ammann M.: Photoenhanced Uptake of Gaseous NO_2 on Solid Organic Compounds: A Photochemical Source of HONO?, Faraday Discuss., 130, 195–210, 2005.

Geyer, A., Alicke, B., Konrad, S., Schmitz, T., Stutz, J., and Platt, U.: Chemistry and oxidation capacity of the nitrate radical in the continental boundary layer near Berlin, J. Geophys. Res., 106, 8013–8025, 2001.

Gutzwiller, L., Arens, F., Baltensperger, U., Gäggeler, H. W., and Ammann, M.: Significance of Semivolatile Diesel Exhaust Organics for Secondary HONO Formation, Environ. Sci. Technol., 36, 677–682, 2002.

Harrison, R. M., Yin, J., Tilling, R. M., Cai, X., Seakins, P. W., Hopkins, J. R., Lansley, D. L., Lewis, A. C., Hunter, M. C., Heard, D. E., Carpenter, L. J., Creasey, D. J., Lee, J. D., Pilling, M. J., Carslaw, N., Emmerson, K. M., Redington, A., Derwent, R. G., Ryall, D., Mills, G., and Penkett, S. A.: Measurement and modelling of air pollution and atmospheric chemistry in the U.K. west midlands conurbation: overview of the PUMA consortium project, Sci. Total Enviro., 360, 5–25, 2006.

Hayman G. D.: Effects of Pollution Control on UV Exposure. AEA Technology Final Report (Ref: AEA/RCEC/22522001/R/002 Issue 1) AEA Technology, Oxfordshire, 1997.

Heard, D. E., Carpenter, L. J., Creasey, D. J., Hopkins, J. R., Lee, J. D., Lewis, A. C., Pilling, M. J., Seakins, P. W., Carslaw, N., and Emmerson K. M.: High levels of the hydroxyl radical in the winter urban troposphere, Geophys. Res. Lett., 31, L18112, 2004.

Heland, J., Kleffmann, J., Kurtenbach, R., and Wiesen, P.: A New Instrument to Measure Gaseous Nitrous Acid (HONO) in the Atmosphere, Environ. Sci.Technol., 35, 3207–3212, 2001.

Holland, F., Hofzumahaus, A., Schäfer, J., Kraus, A., and Pätz, H.-W.: Measurements of OH and HO_2 Radical Concentration and Photolysis Frequencies during BERLIOZ, J. Geophys. Res., 180, 8246, doi:10.1029/2001JD001393, 2003.

Huang, G., Zhou, X., Deng, G., Qiao, H., Civarolo, K.: Measurements of atmospheric nitrous acid and nitric acid, Atmos. Environ., 36, 2225–2235, 2002.

Jenkin, M. E., Saunders, S. M., and Pilling, M. J.: The tropospheric degradation of volatile organic compounds: a protocol for mechanism development, Atmos. Environ., 31, 81–104, 1997.

Johnson, D. and Marston, G.: The gas-phase ozonolysis of unsaturated volatile organic compounds in the troposphere, Chem. Soc. Rev., 37, 699–716, 2008.

Kanaya, Y., Cao, R., Akimoto, H., Fukoda, M., Komazaki, Y., Yokouchi, Y., Koike, M., Tanimoto, H., Takegawa, N., and Konodo, Y.: Urban photochemistry in central Tokyo: 1. Observed and modelled OH and HO_2 radical concentrations during the winter and summer of 2004, J. Geophys. Res., 112, D21312, doi:10.1029/2007JD008670, 2007.

Kleffmann, J., Heland, J., Kurtenbach, R., Lörzer, J. C., and Wiesen, P.: A New Instrument (LOPAP) for the Detection of Nitrous Acid (HONO), Environ. Sci. Technol., 4(4), 48–54, 2002.

Kleffmann, J., Kurtenbach, R., Lörzer, J. C., Wiesen, P., Kalthoff, N., Vogel, B., and Vogel, H.: Measured and simulated vertical profiles of nitrous acid Part I: Field measurements, Atmos. Environ., 37, 2949–2955, 2003.

Kleffmann, J., Gavriloaiei, T., Hofzumahaus, A., Holland, F., Koppmann, R., Rupp, L., Schlosser, E., Siese, M., Wahner, A.: Daytime Formation of Nitrous Acid: A Major Source of OH Radicals in a Forest, Geophys. Res. Lett., 32, L05818, doi:10.1029/2005GL022524, 2005.

Kleffmann, J., Lörzer, J. C., Wiesen, P., Kern, C., Trick, S., Volkamer, R., Rodenas, M., and Wirtz, K.: Intercomparisons of the DOAS and LOPAP Techniques for the Detection of Nitrous Acid (HONO) in the Atmosphere, Atmos. Environ., 40, 3640–3652, 2006.

Kleffmann, J.: Daytime Sources of Nitrous Acid (HONO) in the Atmospheric Boundary Layer,

Chem. Phys. Chem., 8, 1137–1144, 2007.
Kleffmann, J. and Wiesen, P.: Technical Note: Quantification of interferences of wet chemical HONO measurements under simulated polar conditions, Atmos. Chem. Phys. Discuss., 8, 3497–3523, 2008, http://www.atmos-chem-phys-discuss.net/8/3497/2008/.
Koppmann, R., Johnen, F.J., Khedim, A., Rudolph, J., Wedel, A., and Wiards, B.: The influence of ozone on light nonmethane hydrocarbons during cryogenic preconcentration, J. Geophys. Res., 100, 11383–11391, 1995.
Kurtenbach, R., Becker, K. H., Gomes, J. A. G., Kleffmann, J., Lörzer, J. C., Spittler, M., Wiesen, P., Ackermann, R., Geyer, A., and Platt, U.: Investigation of Emissions and Heterogeneous Formation of HONO in a Road Traffic Tunnel, Atmos. Environ., 35, 3385–3394, 2001.
Li, S., Matthews, J., and Sinha, A.: Atmospheric Hydroxyl Radical Production from Electronically Excited NO_2 and H_2O, Science, 319, 1657–1660, 2008.
Mihelcic, D., Holland, F., Hofzumahaus, A., Hoppe, L., Konrad, S., Müsgen, P., Pätz, H.-W., Schäfer, H.-J., Schmitz, T., Volz-Thomas, A., Bächmann, K., Schlomski, S., Platt, U., Geyer, A., Alicke, B., and Moortgat, G.: Peroxy radicals during BERLIOZ at Pabstthum: Measurements, radical budgets and ozone production, J. Geophys. Res., 108(D4), 8254, doi:10.1029/2001JD001014, 2003.
Niedojadlo, A., Becker, K. H., Kurtenbach, R., and Wiesen P.: The contribution of traffic and solvent use to the total NMVOC emission in a German city derived from measurements and CMB modelling, Atmos. Environ., 41(33), 7108–7126, 2007.
Paulson, S. E. and Orlando, J. J.: The reactions of ozone with alkenes: An important source of HO_x in the boundary layer, Geophys. Res. Lett., 23(25), 3727–3730, 1996.
Rappenglück, B., Oyola, P., Olaeta, I., and Fabian, P.: The evaluation of photochemical smog in the metropolitan area of Santiago de Chile, J. Appl. Meteorol., 39, 275–290, 2000.
Rappenglück, B., Schmitz, R., Bauerfeind, M., Cereceda-Balic, F., von-Baer, D., Jorquera, H., Silva, Y., and, Oyola, P.: An Urban Photochemistry study in Santiago de Chile, Atmos. Environ., 39, 2913–2931, 2005.
Ren, X., Harder, H., Martinez, M., Lesher, R. L., Oliger, A., Simpas, J. B., Brune, W. H., Schwab, J. J., Demerjian, K. L., He, Y., Zhou, X., and Gao, H.: OH and HO_2 Chemistry in the Urban Atmosphere of New York City, Atmos. Environ., 37, 3639–3651, 2003.
Ren, X., Brune, W. H., Mao, J., Mitchell, M. J., Lesher, R. L., Simpas, J. B., Metcalf, A. R., Schwab, J.J., Cai, C., Li, Y., Demerjian, K. L., Felton, H. D., Boynton, G., Adams, A., Perry,

J., He, Y., Zhou, X., and Hou, J.: Behavior of OH and HO_2 in the Winter Atmosphere in New York City, Atmos. Environ., 40, S252–S263, 2006.
Rickard, A. R., Johnson, D., McGill, C. D., and Marston, G.: OH yields in the gas-phase reactions of ozone with alkenes, J. Phys. Chem., A103, 7656–7664, 1999.
Rohrer, F. and Berresheim, H.: Strong correlation between levels of tropospheric hydroxyl radicals and solar ultraviolet radiation, Nature, 442, 184–187, doi:10.1038/nature04924, 2006.
Rubio, M. A., Oyola, P., Gramsch E., Lissi, E., Pizzaro, J., and Villena, G.: Ozone and peroxyacetylnitrate in downtown Santiago, Chile, Atmos. Environ., 38, 4931–4939, 2004.
Rubio, M. A., Lissi, E., Villena, G., Caroca, V., Gramsch, E., and Ruiz, A.: Estimation of hydroxyl and hydroperoxyl radicals concentrations in the urban atmosphere of Santiago, J. Chilean Chem. Soci., 50(2), 375–379, 2005.
Rubio, M. A., Zamorano, N., Lissi, E., Rojas, A., Gutierrez, L., and von Bare, D.: Volatile carbonyl compounds in downtown Santiago, Chile, Chemosphere, 62, 1011–1020, 2006.
Saunders, S. M., Jenkin, M. E., Derwent, R. G., and Pilling, M. J.: Protocol for the development of the Master Chemical Mechanism, MCM V3: tropospheric degradation of non-aromatic VOC, Atmos. Chem. Phys., 3, 161–180, 2003, http://www.atmos-chem-phys.net/3/161/2003/.
Sillman, S.: The relation between ozone, NO_x and hydrocarbons in urban and polluted rural environments, Atmos. Environ., 33, 1821–1845, 1999.
Shirley, T. R., Brune, W. H., Ren, X., Mao, J., Lesher, R., Cardenas, B., Volkamer, R., Molina, L. T., Molina, M. J., Lamb, B., Velasco, E., Jobson, T., and Alexander, M.: Atmospheric oxidation in the Mexico City Metropolitan Area (MCMA) during April 2003, Atmos. Chem. Phys., 6, 2753–2765, 2006, http://www.atmos-chem-phys.net/6/2753/2006/.
Sheehy, P. M., Volkamer, R., Molina, L. T., and Molina, M. J.: Oxidative capacity of the Mexico City atmosphere - Part 2: A RO_x radical cycling perspective, Atmos. Chem. Phys. Discuss., 8, 5359–5412, 2008, http://www.atmos-chem-phys-discuss.net/8/5359/2008/.
Spindler, G., Hesper, J., Brüggemann, E., Dubois, R., Müller, T. and Herrmann, H.: Wet Annular Denuder Measurements of Nitrous Acid: Laboratory Study of the Artefact Reaction of NO_2 with S(IV) in Aqueous Solutions and Comparison with Field Measurements, Atmos. Environ., 37, 2643–2662, 2003.
Stemmler, K., Ammann, M., Dondors, C., Kleffmann, J., and George, C.: Photosensitized Re-

duction of Nitrogen Dioxide on Humic Acid as a Source of Nitrous Acid, Nature, 440, 195–198, 2006.

Stemmler, K., Ndour, M., Elshorbany, Y., Kleffmann, J., D'Anna, B., George, C., Bohn, B., and Ammann, M.: Light induced conversion of nitrogen dioxide into nitrous acid on submicron humic acid aerosol, Atmos. Chem. Phys., 7, 4237–4248, 2007, http://www.atmos-chem-phys.net/7/4237/2007/.

Stockwell, W. R., Kirchner, F., Kuhn, M., and Seefeld, S.: A new mechanism for regional atmospheric chemistry modelling, J. Geophys. Res., 102(D22), 25 847–25 880, 1997.

Stutz, J., Alicke, B., and Neftel, A.: Nitrous Acid Formation in the Urban Atmosphere: Gradient Measurements of NO_2 and HONO over Grass in Milan, Italy, J. Geophys. Res., 107(D22), 8192, doi:10.1029/2001JD000390, 2002.

Stutz, J., Alicke, B., Ackermann, R., Geyer, A., Wang, S. H., White, A. B., Williams, E. J., Spicer, C. W., and Fast, J. D.: Relative humidity dependence of HONO chemistry in urban areas, J. Geophys. Res., 109, D03307, doi:10.1029/2003JD004135, 2004.

Vogel, B., Vogel, H., Kleffmann, J., and Kurtenbach, R.: Measured and Simulated Vertical Profiles of Nitrous Acid, Part II – Model Simulations and Indications for a Photolytic Source, Atmos. Environ., 37, 2957–2966, 2003.

Volkamer, R., Sheehy, P. M., Molina, L. T., and Molina, M. J.: Oxidative capacity of the Mexico City atmosphere - Part 1: A radical source perspective, Atmos. Chem. Phys. Discuss., 7, 5365–5412, 2007, http://www.atmos-chem-phys-discuss.net/7/5365/2007/.

Yoshino, A., Sadanagab, A., Watanabea, K., Katoa, S., Miyakawaa, Y., Matsumotoc, J., and Kajiia, Y.: Measurement of total OH reactivity by laser-induced pump and probe technique-comprehensive observations in the urban atmosphere of Tokyo, Atmos. Environ., 40, 7869–7881, 2006.

Zhou, X., Civerolo, K., Dai, H., Huang, G., Schwab, J., and Demerjian, K.: Summertime Nitrous Acid Chemistry in the Atmospheric Boundary Layer at a Rural Site in New York State, J. Geophys. Res., 107(D21), 4590, doi:10.1029/2001JD001539, 2002.

Zhou, X., Gao, H., He, Y., Huang, G., Bertman, S. B., Civerolo, K., and Schwab, J.: Nitric Acid Photolysis on Surfaces in Low-NO_x Environments: Significant Atmospheric Implications, Geophys. Res. Lett., 30(23), 2217, doi:10.1029/2003GL018620, 2003.

Table 1. Instrumentations used during the Santiago de Chile field campaign.

Species	Method	Response time	Detection limit
HONO	LOPAP-technique (Long-Path-Absorption Photometer)	4 min	3 pptv
HCHO	Hantzsch reaction based instrument, Aero Laser CH_2O analyser (Model AL4001)	3 min	50 pptv
NO	Chemiluminescence based analyzer with molybdenum converter (Model TELEDYNE 200 E)	<10 s	400 pptv
NO_2	DOAS-OPSIS optical system	2 min	0.5 ppbv
O_3[a]	Short-path UV absorption (λ=254 nm), from Advanced Pollution Instruments Model 400.	10 s	1 ppbv
O_3[b]	UV absorption based monitor (Dasibi Model 1009-Cp)	10 s	1 ppbv
CO[a]	IR absorption based monitor (Interscan 4000)	20 s	1 ppb
PAN	GC-ECD (Meteorolgie Consult GmbH)	10 min	25 pptv
$j(NO_2)$, $j(O^1D)$	Filter radiometers (Meteorolgie Consult GmbH)	1 min	–
C_3-C_{10} NMHCs	GC-FID analysis (HP Model 6890) following the US Compendium Method TO-17 (EPA)	3 h (day) and 6 h (night)	37 pptv (4–77 pptv)

[a] Measured at the Park O'Higgins station (POH) 1.8 km southeast of the USACH measurement site.
[b] Used to investigate the ozone interferences during the VOC sampling process.

ACPD
8, 19123–19171, 2008

Table 2. List of the VOCs measured during the summer campaign in Santiago de Chile.

MCM	Compound name	D_L (ppbv)	Mixing ratio (ppbv)		
			Max	Average	Median
*	propene	0.07	38.8	3.80	1.56
*	propane	0.07	475	41.8	11.5
*	i-butane (2-methylpropane)	0.06	18.0	2.95	1.57
	1-butene, i-butene	0.20	9.2	2.35	2.04
*	1,3-butadien	0.06	0.41	0.15	0.12
*	n-butane	0.04	18.3	3.89	2.32
*	trans-2-butene	0.04	0.86	0.18	0.11
*	cis-2-butene	0.04	0.67	0.16	0.10
*	3-methyl-1-butene	0.05	1.22	0.19	0.14
*	i-pentane (2-methylbutane)	0.06	27.6	5.75	4.08
*	1-pentene	0.01	1.77	0.30	0.18
	n-pentane, 2-methyl-1-butene	0.06	18.8	2.03	0.82
*	isoprene	0.02	1.84	0.67	0.51
*	trans-2-pentene	0.01	1.41	0.24	0.14
*	cis-2-pentene	0.004	0.74	0.15	0.10
*	2-methyl-2-butene	0.04	2.10	0.33	0.20
	2,2-dimethylbutane	0.09	5.20	1.07	0.63
	cyclopentene	0.02	0.17	0.05	0.04
	methyl-tert-butyl ether, 2,3-dimethylbutan, cyclopentan	0.16	5.84	1.28	0.89
	2-methylpentane	0.06	14.4	3.11	1.94
*	3-methylpentane	0.05	6.09	1.40	0.92
*	1-hexene	0.02	0.80	0.20	0.14
	n-hexan, 2-ethyl-1-butene	0.06	5.31	1.36	0.94
	2,3-dimethyl-1,3-butadiene	0.02	0.15	0.05	0.03
	methylcyclopentane, 1-methyl-1-cyclopentene	0.07	6.27	1.36	0.87
*	2,3-dimethyl-2-butene	0.02	0.52	0.10	0.06
*	benzene	0.08	9.22	2.13	1.43

* Compounds included in the MCM model (see Sect. 3.5).

ACPD
8, 19123–19171, 2008

Table 2. Continued.

MCM	Compound name	D_L (ppbv)	Mixing ratio (ppbv)		
			Max	Average	Median
	cyclohexane, 2,3-dimethylpentane	0.07	8.07	2.08	1.50
*	2-methylhexane	0.04	1.71	0.35	0.22
	cyclohexene	0.05	0.39	0.13	0.10
	1-heptene	0.02	1.01	0.24	0.17
	2,2,4-trimethylpentane	0.03	3.81	0.92	0.68
*	n-heptane	0.02	2.50	0.55	0.42
	1,4-cyclohexadiene	0.04	0.14	0.07	0.06
	2,3,4-trimethylpentane	0.03	0.92	0.13	0.05
*	toluene	0.01	32.7	6.30	4.11
	2-methylheptane	0.03	1.46	0.31	0.21
	3-methylheptane	0.02	0.57	0.10	0.07
	4-methylheptane, 1-methyl-1-cyclohexene	0.06	1.57	0.30	0.19
	1-octene	0.03	0.80	0.18	0.14
*	n-octane	0.02	1.82	0.34	0.23
*	ethylbenzene	0.02	6.06	1.38	1.14
	m-& p-xylene	0.04	22.2	5.14	4.26
*	styrene	0.03	1.02	0.22	0.16
*	o-xylene	0.04	7.72	1.81	1.50
*	$\alpha-$pinene	0.07	1.95	0.41	0.27
*	n-propylbenzene	0.02	1.68	0.36	0.26
*	4-ethyltoluene	0.01	1.40	0.30	0.21
*	1,3,5-trimethylbenzene	0.03	2.79	0.58	0.38
*	n-decane	0.02	2.94	0.60	0.42
	1,2,4-trimethylbenzene, tet. butylbenzene	0.04	6.91	1.42	0.92
*	1,2,3-trimethylbenzene	0.01	1.31	0.27	0.17
	1,2,3,4-tetramethylbenzene	0.02	5.55	0.43	0.22

ACPD
8, 19123–19171, 2008

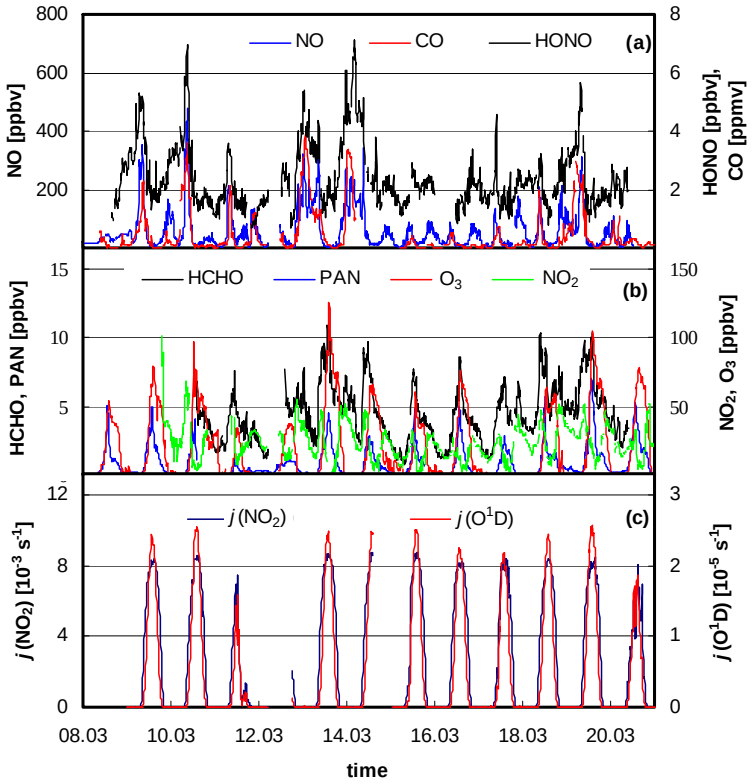

Fig. 1. 10 min average data of HONO, NO, CO, HCHO, NO_2, O_3, $j(NO_2)$ and $j(O^1D)$ during the field campaign in Santiago de Chile, 8–20 March 2005.

ACPD
8, 19123–19171, 2008

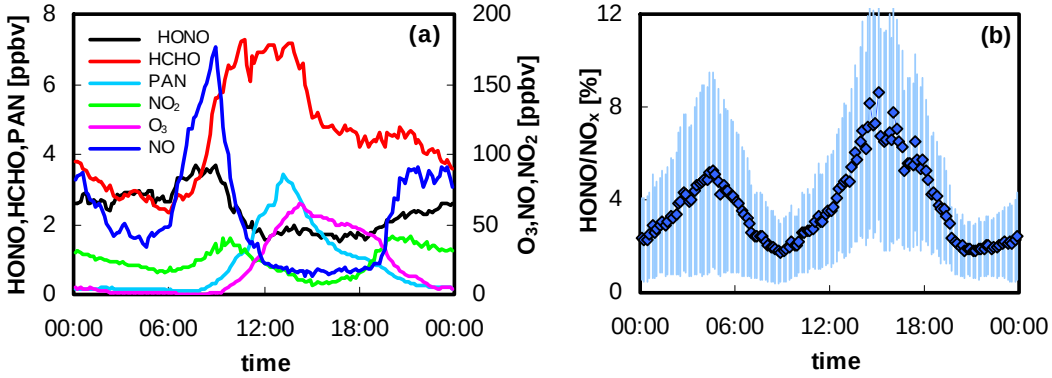

Fig. 2. **(a)** Average diurnal 10 min data of HONO, NO, NO_2, PAN, O_3 and HCHO and **(b)** average diurnal HONO/NO_x ratio.

ACPD
8, 19123–19171, 2008

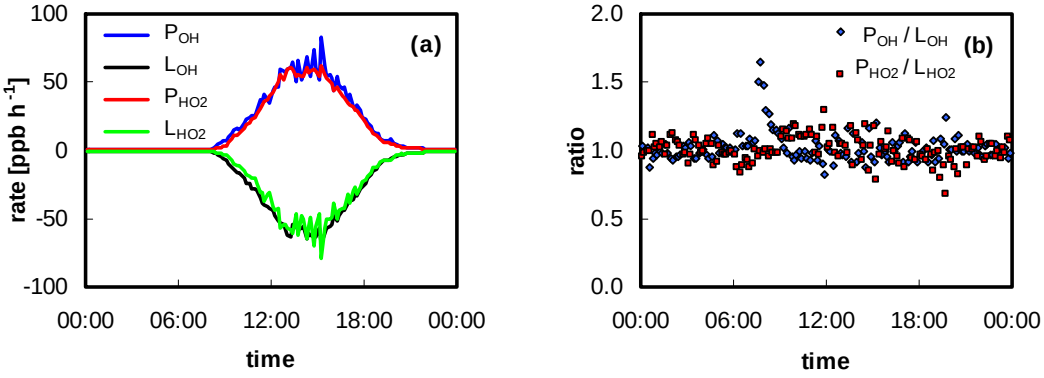

Fig. 3. (a) Production and destruction rates of OH and HO_2. **(b)** Ratio of the rates of production to destruction of OH and HO_2.

ACPD

8, 19123–19171, 2008

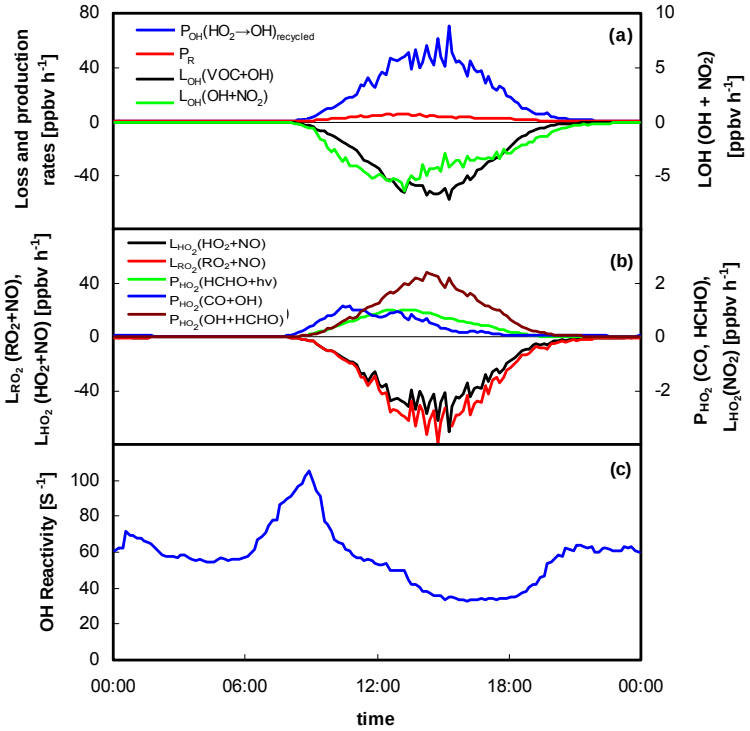

Fig. 4. Production and destruction rates of **(a)** OH and **(b)** HO_2 and **(c)** modelled OH reactivity.

ACPD
8, 19123–19171, 2008

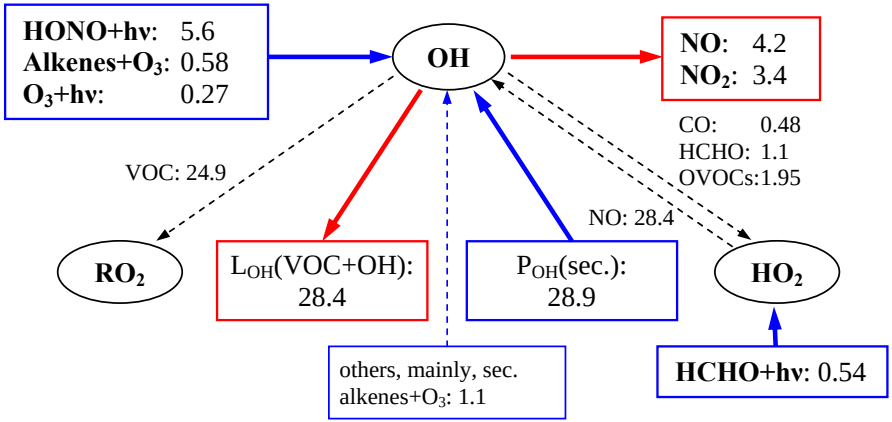

Fig. 5. Average daytime (8–19 h) fluxes of the net radical sources and sinks as calculated by the MCM model. Units are in ppbv h^{-1}. HONO net contribution (~52%) in this diagram is slightly lower than in the text because $[HONO]_{PSS}$ is calculated here using [OH] calculated by the MCM (~4% higher).

ACPD
8, 19123–19171, 2008

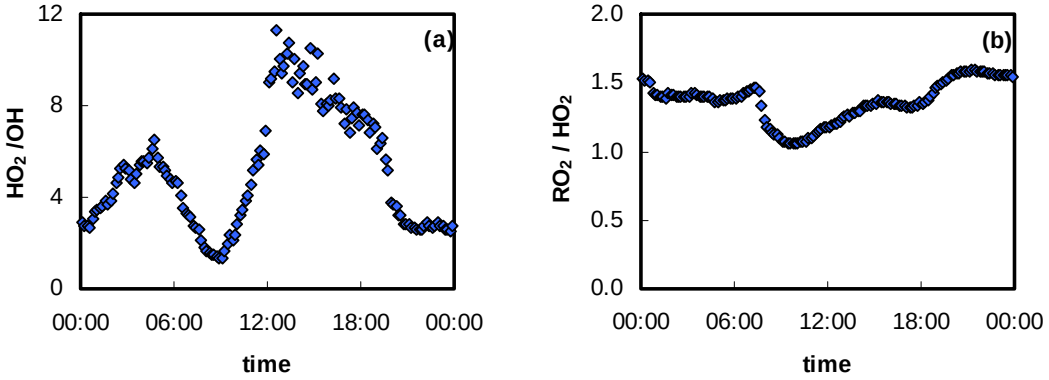

Fig. 6. Average MCM model diurnal variation of **(a)** HO_2/OH ratio and **(b)** RO_2/HO_2 ratio.

ACPD
8, 19123–19171, 2008

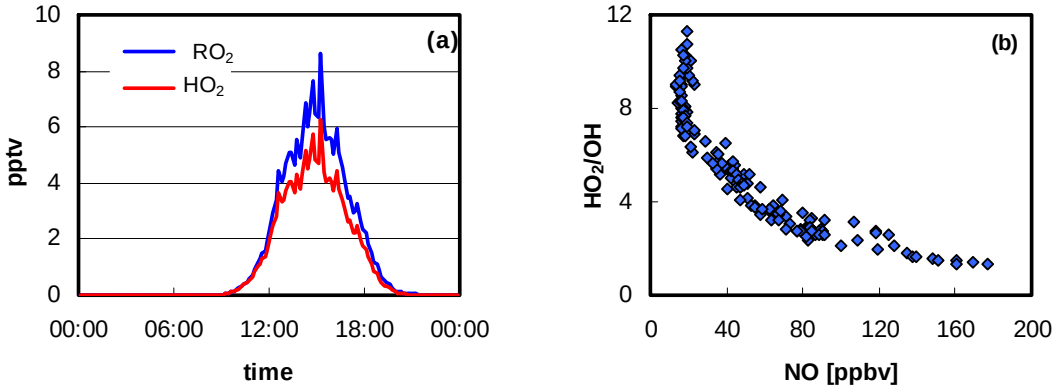

Fig. 7. (a) Average MCM model diurnal variation of HO_2 and RO_2. **(b)** HO_2/OH ratio vs. NO.

ACPD
8, 19123–19171, 2008

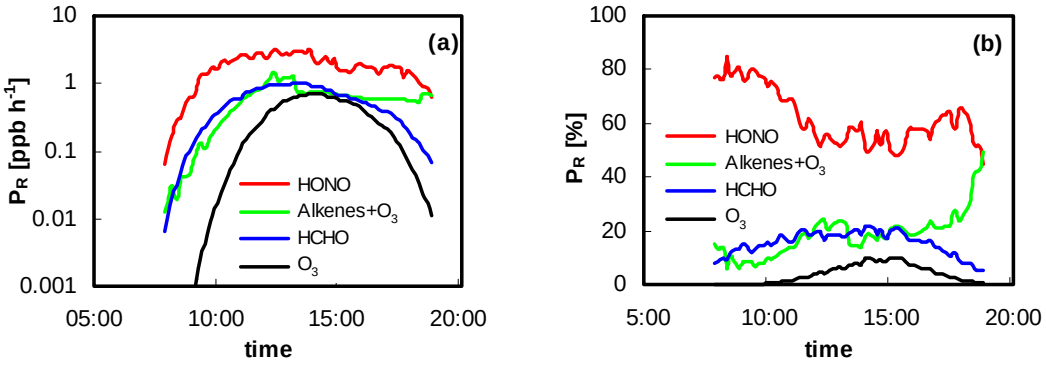

Fig. 8. Average absolute **(a)** and relative **(b)** diurnal daytime radical production rates (P_R).

ACPD
8, 19123–19171, 2008

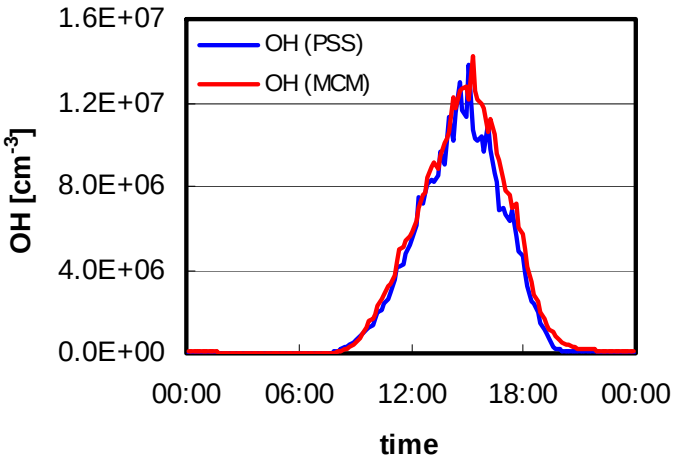

Fig. 9. Average diurnal variation of OH concentration calculated by both the MCM and PSS.

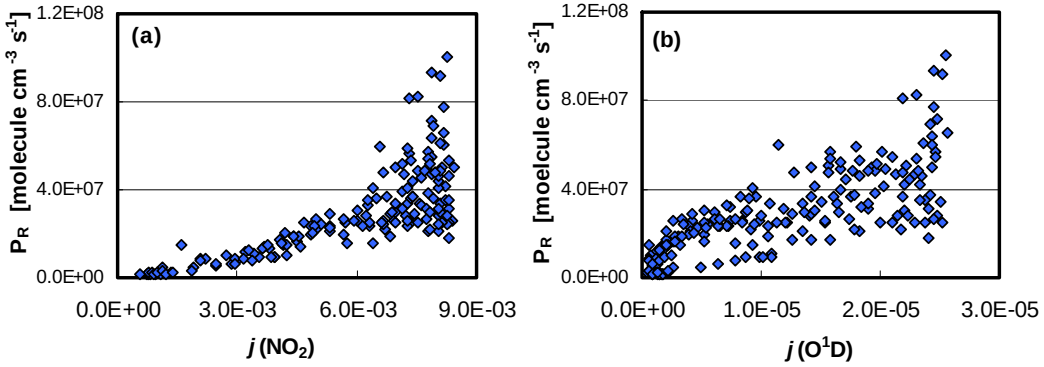

Fig. 10. Correlations between the radical production rate, P_R and **(a)** $j(NO_2)$ and **(b)** $j(O^1D)$.

ACPD
8, 19123–19171, 2008

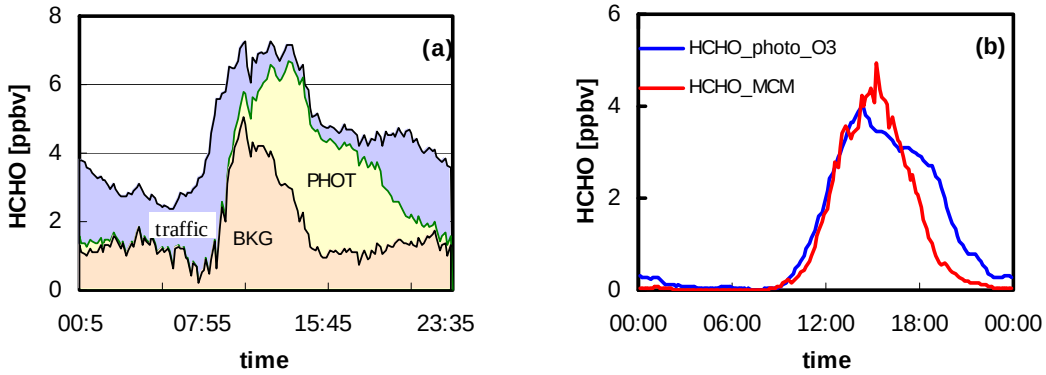

Fig. 11. (a) HCHO source apportionment, **(b)** Photochemical HCHO simulated with MCM and calculated with O_3 tracer.

ACPD
8, 19123–19171, 2008

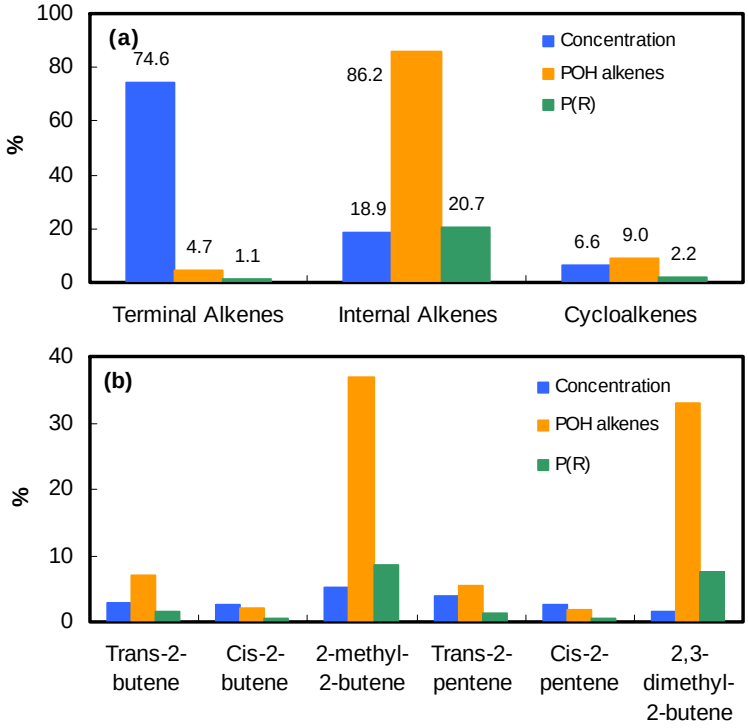

Fig. 12. Contributions of **(a)** different alkenes and **(b)** internal alkenes to the OH production.

ACPD
8, 19123–19171, 2008